

We are IntechOpen, the world's leading publisher of Open Access books Built by scientists, for scientists

6,900

Open access books available

186,000

International authors and editors

200M

Downloads

Our authors are among the

154

Countries delivered to

TOP 1%

most cited scientists

12.2%

Contributors from top 500 universities



WEB OF SCIENCE™

Selection of our books indexed in the Book Citation Index
in Web of Science™ Core Collection (BKCI)

Interested in publishing with us?
Contact book.department@intechopen.com

Numbers displayed above are based on latest data collected.
For more information visit www.intechopen.com



Photoacoustic Imaging of the Eye

Yanxiu Li and Yannis Mantas Paulus

Abstract

Photoacoustic imaging (PAI) is a novel, hybrid, non-ionizing, and non-invasive imaging technology with high-resolution, high sensitivity, high-contrast, and high depth of penetration. Hence, it has particularly useful applications in eye investigations. It can provide both anatomic and functional ocular characterizations. Many eye diseases, including macular degeneration and diabetic retinopathy, involve abnormalities in the vasculature, and thus the ability of PAI to affectively visualize the vasculature can be incredibly helpful to evaluate normal and disease states of the eye. In future research, PAI of the eye can be dramatically improved in terms of its resolution, use of contrast agents for molecular imaging, safety evaluations to develop a clinically approved system, and integration with existing fundus imaging modalities. Multimodality ocular imaging platforms have also been successfully developed by a combination of photoacoustic microscopy (PAM) with other optical imaging such as optical coherence tomography (OCT), scanning laser ophthalmoscopy (SLO), and fluorescence microscopy (FM). The multimodal images can accurately be acquired from a single imaging system and co-registered on the same image plane, enabling improved evaluation of eye disease states. In this book chapter, the potential application of photoacoustic imaging of the eye in both research and clinical diagnosis are comprehensively discussed as a powerful medical screening technique for visualization of various ocular diseases.

Keywords: photoacoustic imaging, photoacoustic ophthalmoscopy, photoacoustic microscopy, multimodal imaging

1. Introduction

The eye is unique organ in that it is optically transparent to visible light in normal health and thus offers optical access to internal structures. The refractive system of the normal eye includes the cornea, the fluid-filled anterior chamber, crystalline lens, and gel-like vitreous. These optically transparent structures have low absorption and light scattering to visible light, which plays a pivotal role in the entry of light and the formation of visual pathways. In the eye, the major endogenous light-absorbing materials are hemoglobin and melanin. Hemoglobin is present in blood vessels in the iris, choroid, ciliary body, retina, conjunctiva, and pathologic neovascularization. Melanin is present inside the uvea (iris, choroid and ciliary body), retinal pigment epithelium (RPE) and pigmented tumors.

Photoacoustic imaging (PAI), which converts light energy into sound waves, has been demonstrated to image hemoglobin [1, 2] and melanin [3, 4]. Thus eyes are an ideal system for PAI. PAI can provide an ocular vascular image based on the inherent optical absorbance of hemoglobin. Many eye diseases, including corneal neovascularization, macular degeneration, diabetic retinopathy, sickle cell

retinopathy, and retinal vein occlusions, involve abnormalities in the vasculature. Thus the unique ability of PAI to provide detailed vascular morphologic information can assist ophthalmic diagnosis.

Currently several imaging modalities have been used to diagnose and monitor ocular diseases. Well-established imaging instruments include color fundus photography, ultrasound (US) imaging, fluorescein angiography (FA), indocyanine green angiography (ICGA), scanning laser ophthalmoscopy (SLO), optical coherence tomography (OCT) and OCT angiography (OCTA). Each imaging modality has advantages and disadvantages. OCT has a limited depth of penetration and has difficulty visualizing deep structures like the choroid and sclera. FA and ICGA require the use of an exogenous contrast agent that may cause adverse reactions and cannot specify the depth of the vessels. OCTA is unable to show leakage, provides limited view of microaneurysms, has a limited depth of penetration, and has a restricted field of view often with motion artifacts.

PAI is a new, emerging, non-ionizing and non-invasive imaging technology. PAI is based on the optical absorption contrast so that can provide anatomical information and functional analysis for the eye as well as with a high depth of penetration. In 2010, photoacoustic imaging was first described in the eye of a living animal [4]. Since then, there is a huge advance in photoacoustic imaging of the eye. Furthermore, the application of multimodality imaging systems including integrated photoacoustic microscopy (PAM) with other imaging modalities and the use of contrast agents for molecular imaging have undergone significant development. This chapter focuses on recent advances and applications of photoacoustic imaging of the eyes.

2. Photoacoustic imaging of the eye

Photoacoustic imaging systems can be divided into several categories which include: optical-resolution photoacoustic microscopy (OR-PAM), acoustic-resolution photoacoustic microscopy (AR-PAM), photoacoustic computed tomography (PACT), photoacoustic tomography (PAT) [5, 6]. Ocular PAI systems are primarily OR-PAM and AR-PAM systems due to the importance of high resolution imaging in the eye [7–9]. AR-PAM is used to image deep-tissues, where an illumination laser is diffusively delivered to the tissue and a focused acoustic detector is used to detect the induced PA signals. The lateral resolution of AR-PAM is determined by the acoustic focus spot, and the axial resolution is determined by the acoustic center frequency and bandwidth [5, 8]. OR-PAM has a tighter optical focus than AR-PAM and can achieve micrometer-level lateral resolution. The lateral resolution of OR-PAM is determined by the optical focal spot, and the axial resolution is still determined by the acoustic parameters [5, 8].

PAI can also be classified into mechanical-scanning systems and optical-scanning imaging systems [7]. In the mechanical-scanning mode, both the optical excitation and ultrasound transducer are simultaneously scanned over a planar surface. Each step of the scan can detect and generate a PA signal. During imaging, a water tank is necessary to maintain ultrasound coupling [6]. The mechanical-scanning can be used to visualize almost all the eye tissues, including the cornea, iris, lens, retina, choroid, sclera, and blood vessels [4]. In the optical-scanning mode, the focused optical illumination is raster-scanned using galvanometers, while the ultrasound transducer is kept stationary [10]. **Figure 1a** shows the schematic diagram of the optical-scanning in a multimodality system. **Figure 1b** illustrates the physical setup [11]. Compared with mechanical-scanning, optical-scanning can provide higher scanning speed, and it is suitable for chorioretinal microvasculature imaging, and compatibility with OCT and SLO [9, 12].

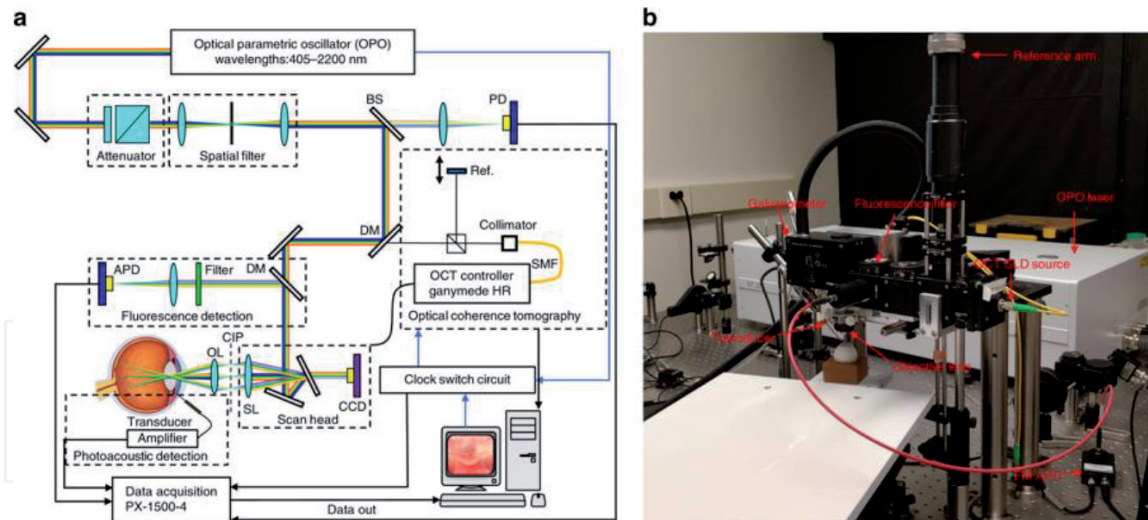


Figure 1. Integrated multimodal PAM, OCT, and FM imaging system. (a) Schematic. (b) Photograph of the multimodality retinal and choroïdal imaging system. OPO, optical parametric oscillator; SLD, superluminescent diode; BS, beam splitter; DM, dichroic mirror; SL, scan lens; OL, ophthalmic lens; CIP, conjugate image planes. Adapted with permission from Ref. [11] [Publisher: Springer Nature].

Currently, many applications of ocular PAI have been reported. This chapter summarizes those applications by the anatomic portion of the eye imaged and functional information.

2.1 PA imaging of the anterior segment vasculature of the eye

2.1.1 Normal iris vasculature

Anterior segment PA imaging of a normal eye receives signal from hemoglobin in the red blood cells of the iris microvasculature. Both AR-PAM and OR-PAM have been reported for iris vascular imaging. de la Zerda et al. [4] have used AR-PAM to qualitatively assess the rabbit eye *in vivo*. PA signals from the iris were detected, but the image of iris microvasculature was not clearly as the lateral resolution of the system was limited (around 200 μm). Hu et al. [13] have used a OR-PAM mechanical scanning system to get high resolution *in vivo* images of the iris microvascular in Swiss Webster albino mice (**Figure 2a**). The lateral resolution of the system was $\sim 5 \mu\text{m}$. The center frequency of the focused ultrasonic detector was 75 MHz. Hu et al. also have used two excitation wavelengths (570 and 578 nm) to estimate the concentrations of oxyhemoglobin (HbO_2) and deoxyhemoglobin (HbR), thereby have quantitatively measured sO_2 of the iris microvasculature. Dashed box in (**Figure 2a**) show the false-color map of the vasculature. With the limitation of mechanical scanning, the image acquisition took ~ 2 hours. Rao et al. [15] have used an OR-PAM hybrid-scanning system to image the major artery circle and the minor artery circle of the iris microvasculature in albino mice. Zhao et al. [14] have used a custom-built OR-PAM system to perform three-dimensional (3-D) vasculature imaging of rat iris *in vivo* with a lateral resolution of $\sim 5 \mu\text{m}$. They have extracted accurately vessel diameter, vascular density, and vascular tortuosity information (**Figure 2b**).

2.1.2 Corneal neovascularization

Normal corneal tissue is avascular and optically transparent. Corneal neovascularization is a pathologic condition that can lead to reduced vision characterized by the

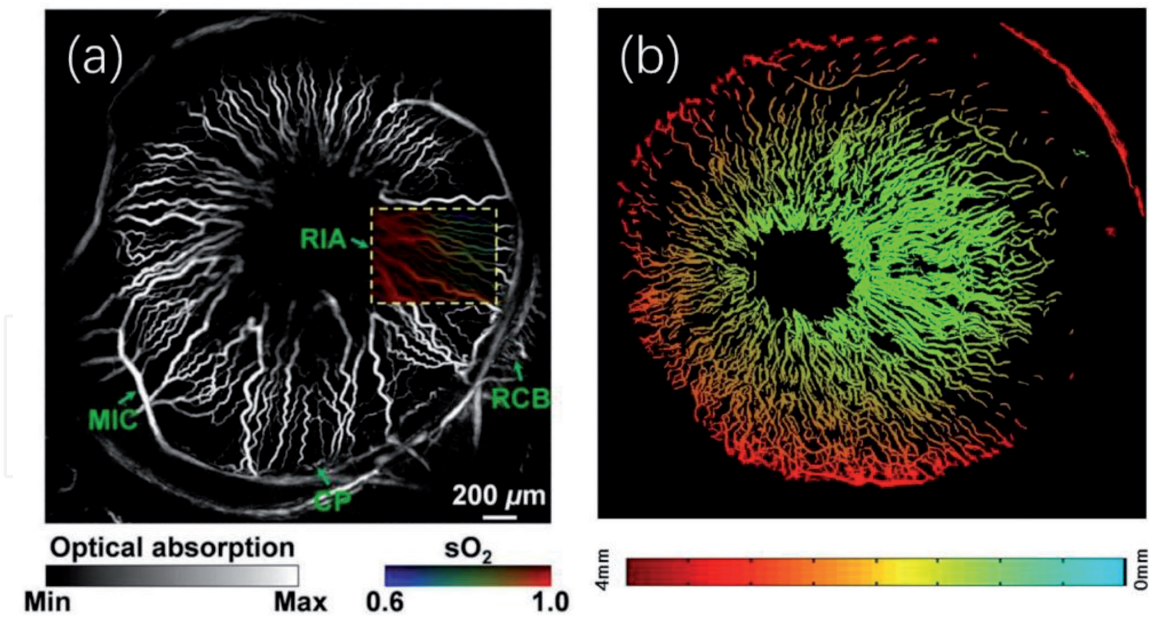


Figure 2.

PA images of the iris vasculature. (a) Label-free photoacoustic ophthalmic angiography of hemoglobin oxygen saturation sO_2 in the iris microvasculature of a living adult Swiss Webster mouse. CP, ciliary process; MIC, major iris circle; RCB, recurrent choroidal branch; RIA, radial iris artery. Adapted with permission from Ref. [13] [Publisher: The Optical Society (OSA)]. (b) Depth encoded photoacoustic imaging results of iris vasculature. Reproduced with permission from [14] [Publisher: SPIE].

presence of blood vessels in the cornea. This pathophysiology has been observed in humans with inflammatory or autoimmune responses.

Liu et al. [16] have used a mechanical scanning OR-PAM system to image corneal neovascularization of alkali-burn-injured mouse eyes *in vivo* for the first time. The lateral resolution of the system is 2.76 μm , and the axial resolution is around 50 μm . OR-PAM can achieve a similar lateral resolution as confocal microscopy without a contrast agent. However, the imaging depth is limited (700 μm) and the depth of variation of corneal vessels can be more than 1.4 mm owing to the curvature of the mouse cornea. Jeon et al. [17] have demonstrated a new method to evaluate blood circulation in the eye by combining *in vivo* PAM imaging. By using a machine learning algorithm, random sample consensus algorithm (RANSAC), they could have visualize the PA anterior ocular vasculature image and demonstrate layer-by-layer analysis of corneal neovascularization on a mouse eye (**Figure 3c–e**). This OR-PAM system had a 3 μm lateral resolution. PAM provides the ability to delineate corneal neovascularization from iris vessels and enables visualization of individual capillaries with high-resolution (**Figure 3b**). By stimulating corneal angiogenesis with an alkali burn in Tie2-GFP fluorescent-reporter mice, Kelly-Goss et al. [18] have used the PAM system to analyze functional hemodynamic changes in microvessels over time during adult corneal angiogenesis. These functional measurements of the microvasculature supplement traditional metrics of vascular architecture, including blood flow velocity, hemoglobin content, and sO_2 . The study is the first time to measure the functional information on corneal neovascularization.

Several of the above studies of the anterior segment vasculature images have utilized mechanical scanning OR-PAM system. However, mechanical scanning OR-PAM has limitations: the imaging speed is slow and careful coupling medium is required. Recently, a non-interferometric photoacoustic remote sensing microscopy system has been developed with a high scan rate and an improved signal-to-noise (SNR).

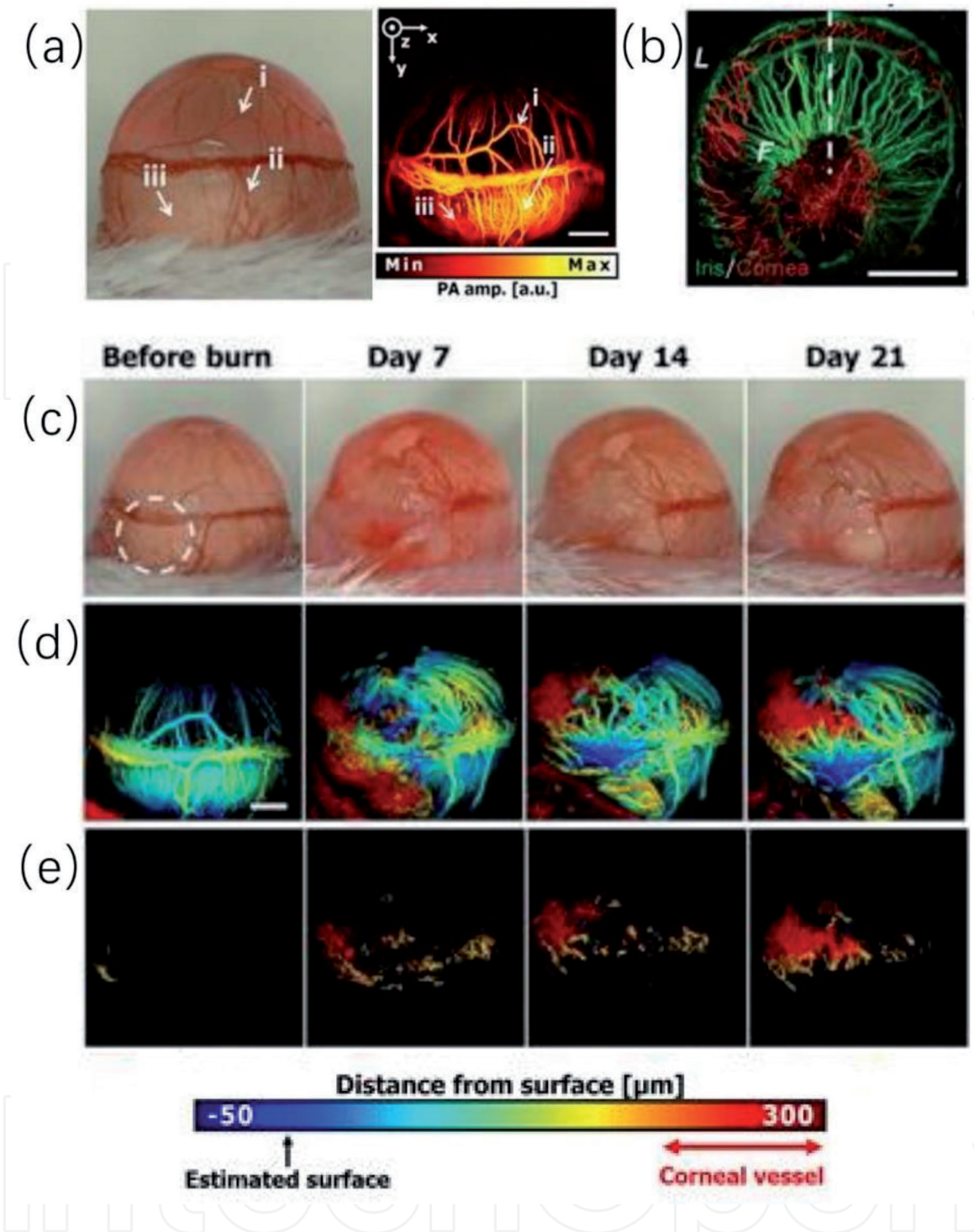


Figure 3. PA images of the corneal neovascularization. (a) Photograph (left) and PA maximum intensity projection (MIP) image (right) of a mouse eye. Adapted with permission from Ref. [17] [Publisher: Springer Nature]. (b) PAM distinguishes between the iris (green) and corneal (red) vasculatures, due to their different depths. Adapted with permission from Ref. [18] [Publisher: Springer Nature]. (c–e) PA imaging of corneal neovascularization on a mouse alkali burn model eye. (c) Representative photographic images taken before alkali burn and 7, 14, and 21 days after alkali burn, the region of burn is highlighted with a white dashed circle. (d) Surface-based depth-encoded images. (e) Images after supra surface vessel isolation from the surface-based depth-encoded images. Scale bars indicate (a, c–e) 500 μm , (b) 50 μm . Adapted with permission from Ref. [17] [Publisher: Springer Nature].

2.2 PA imaging of the posterior segment vasculature of the eye

2.2.1 Retinal vasculature

Posterior segment PAI of a normal eye images red blood cells in the retinal and choroidal microvasculature. To obtain the images, both AR-PAM and OR-PAM

systems have been used, along with mechanical scanning and optical scanning systems.

Using an AR-PAM system, de la Zerda et al. [4] have used a pulsed laser (wavelength 740 nm) combined with a 25 MHz central frequency transducer to mechanically scan a living rabbit eye. They have obtained the blood distribution of the posterior eye. But owing to the system's lateral resolution of 200 μm , limited features of the retinal or choroidal vasculature are visualized. Furthermore, it took 90 min to acquire the full 3-D image.

Jiao et al. [12] have developed an optical-scanning OR-PAM system for *in vivo* retinal imaging in 2010, which they have referred to as a photoacoustic ophthalmoscopy (PAOM). The pigmented rat fundus was imaged using the PAOM system (**Figure 4a–c**). In the PAOM system, the illumination source was a 532 nm pulse laser, the laser pulse energy was set lower than 40 nJ/pulse. The laser induced PA waves from the retina were detected by a custom-built needle ultrasonic transducer (30 MHz; bandwidth: 50%), which was placed in contact with the eyelid coupled by ultrasound gel. The lateral and axial resolution of the PAOM were ~ 20 and 23 μm , respectively. It only took 2.7 s for the volumetric PAOM images consisting of 256 B-scans. Multiple additional studies of imaging retinal vasculature by PAOM in small animals have been performed [10, 20–22]. PAOM as a non-invasive, 3-D microscopic imaging modality, has achieved high-speed, high-resolution *in vivo* imaging of the vasculature of the retina.

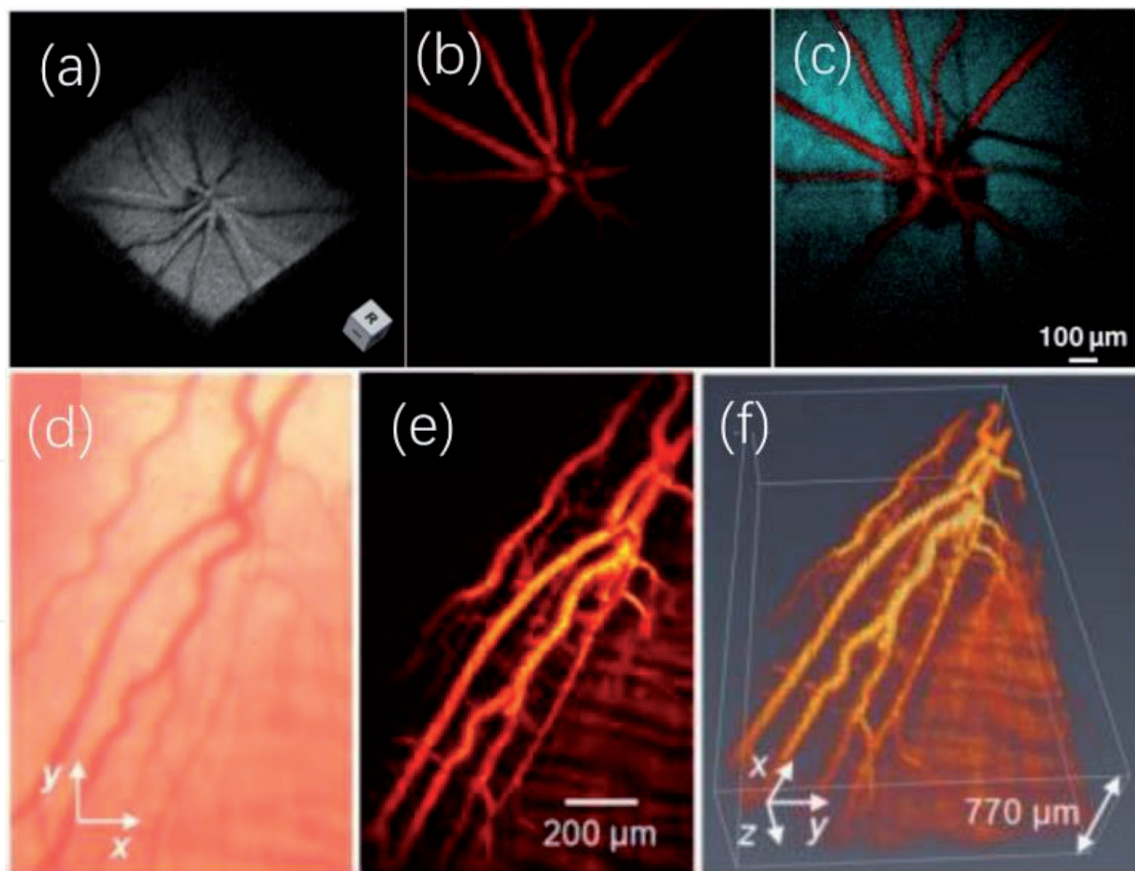


Figure 4.

Retinal vasculature imaging by optical-scanning OR-PAM system. (a–c) PA imaging of retinal vasculature in a rat eye. (a) Showing the imaged retinal structure by PAOM. (b) Segmented PAOM images of the retinal blood vessels. (c) Pseudo-colored PAOM images of the retinal vessels and RPE. Adapted with permission from Ref. [12] [Publisher: The Optical Society (OSA)]. (d–f) PA imaging of an albino rabbit retinal blood vessels. (d) Close-up of the retinal vessels of rabbit. (e) Maximum intensity projections of PAM signals of RVs and choroidal vessels. (f) 3D volumetric rendering of the PAM image. Adapted with permission from Ref. [19] [Publisher: The Optical Society (OSA)].

Before 2017, most reported PAM imaging of the posterior segment used small animals, like mice and rats. Mice have an axial length of ~3 mm and rats ~6 mm, which is much smaller than the human axial length of ~23 mm. In order to improve clinical translation of the technology, Tian et al. [19] have developed a novel PAM system to visualize rabbit chorioretinal vasculature. Rabbit eyes have an axial length of 18.1 mm [23], which is almost 80% of the axial length of human eyes. They have used a 570 nm pulsed laser. The excited PA signals have been captured by a custom-built needle-shaped ultrasonic transducer (27 MHz; bandwidth: 60%) placed in contact with the conjunctiva by ultrasound gel. The laser pulse energy on the rabbit cornea was 80 nJ or half the ANSI safety limit [24]. The lateral and axial resolution of the PAM system were 4.1 and 37 μm , respectively. This PAM system obtains high-resolution images of New Zealand rabbit retinal and choroidal vasculature (**Figure 4d–f**).

2.2.2 Choroidal vasculature

Wei et al. [25] have first applied an OCT-guided PAOM system to image the choroidal vessels in albino rats. The laser output optical wavelength was 578 nm, and the laser pulse energy was set below 40 nJ. The induced PA waves were detected by a custom-built, unfocused needle ultrasonic detector (35 MHz; bandwidth: 50%). The lateral resolution of PAOM was around 20 μm and the axial resolution of PAOM was 23 μm . Based on the OCT cross-sectional images, the distance from the retinal vessel layer to the choroid was found to be 200 μm [26]. Thus, the retinal and choroidal vessels were well resolved along the axial direction. **Figure 5a–c** show PAOM images of segmented retinal vessels and choroidal vessels. Song et al. [20, 27] have used an integrated PAOM and OCT system to detect *in vivo* posterior segment imaging of albino and pigmented rats. They have acquired both retinal and choroidal vessels from an albino rat by PAOM, but they were unable to visualize choroidal vessels from a pigmented rat due to melanin from the retinal pigment epithelium (RPE). **Figure 5d** and **e** show the contrast images. In addition, **Figure 5f** and **g** show the images of choroidal vessels in albino rabbit obtained by Tian et al. [19]. These experimental results have demonstrated that PAI can visualize the choroid and retinal vessels. However, PAM was limited to albino animals when imaging the choroid. The high melanin concentration of the RPE present in front of choroidal vasculature did not allow the illumination light within the visible spectrum range to penetrate through the RPE to generate sufficient PA signal from the choroid for imaging. Near infrared (NIR) light may be a solution to allow PAOM to image choroidal vessels in pigmented eyes.

2.2.3 Retinal neovascularization

Retinal neovascularization (RNV) is the growth of abnormal new retinal blood vessels and represents a major cause of vision loss and blindness. RNV is a common complication of several retinal diseases, including proliferative diabetic retinopathy (PDR), retinal vein occlusions (RVO), sickle cell retinopathy, and retinopathy of prematurity (ROP).

Zhang et al. [11] have demonstrated an integrated PAM, OCT, and fluorescence microscopy (FM) multimodality system to evaluate RNV *in vivo* in rabbit eyes. The model of RNV was induced by intravitreal injection of vascular endothelial growth factor (VEGF), which mimics numerous retinal diseases, such as PDR. Using a similar PAM system as Tian et al. in 2017 but with a laser wavelength of 532 nm, this study has presented high-quality visualization of retinal vasculature and RNV in

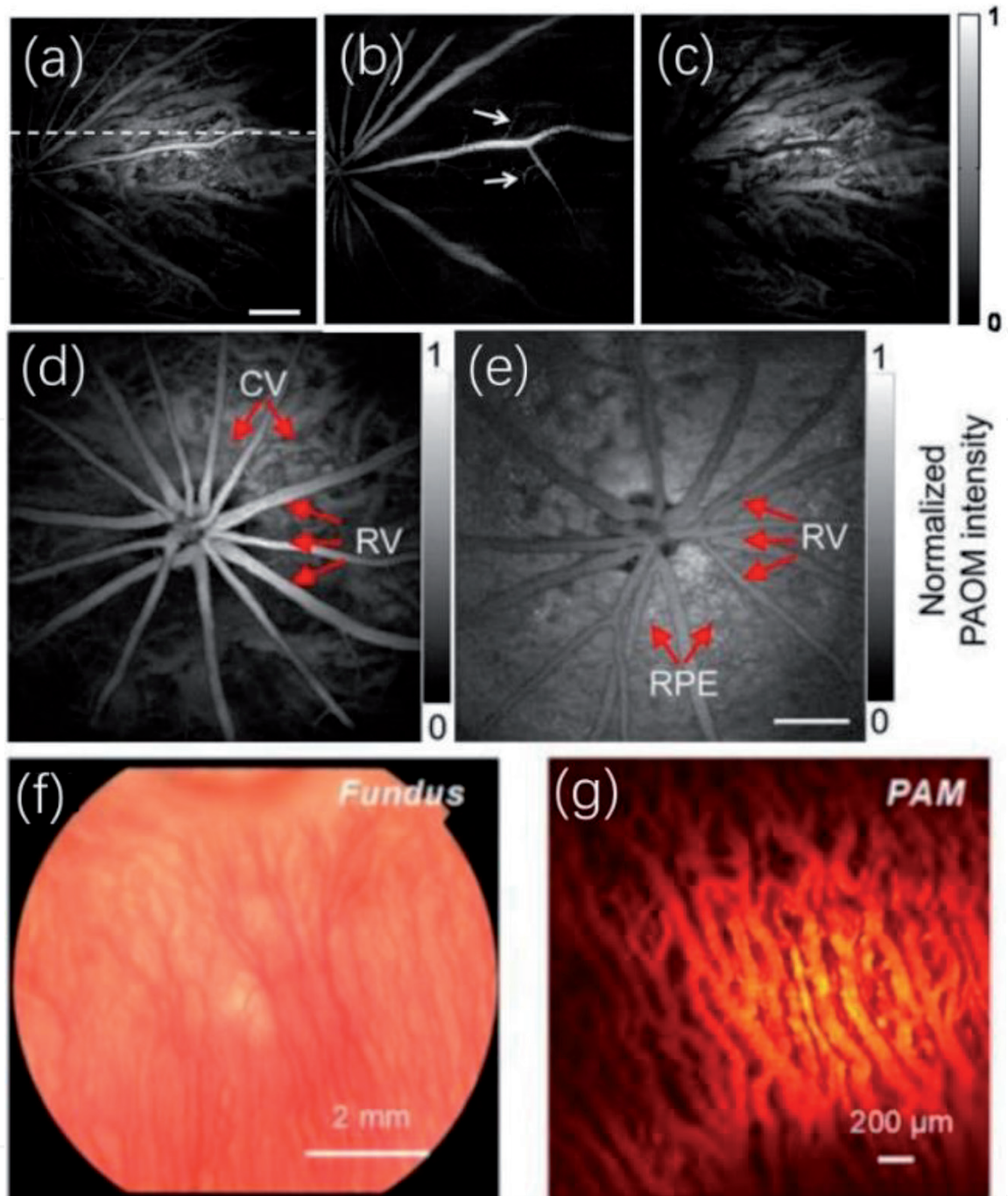


Figure 5. PA images of the chorioretinal vasculature. (a–c) PA imaging of chorioretinal vessel in an albino rat eye. (a) Complete chorioretinal vessel network image. (b) Segmented retinal vessels. (c) Segmented choroidal vessels [25]. (d, e) Comparing PA images of the chorioretinal vasculature in an albino rat and a pigmented rat. (d) Acquired from an albino rat, and (e) acquired from a pigmented rat. RV: retinal vessel; CV: choroidal vessel; RPE, retinal pigment epithelium. Scale bars indicate 500 μm adapted with permission from Ref. [27] [Publisher: JoVE]. (f, g) PA imaging of an albino rabbit. (f) Fundus photograph of rabbit demonstrating the choroidal vessel distribution inferior to the optic nerve. (g) Maximum intensity projections of PAM signals of the CVs. Adapted with permission from Ref. [19] [Publisher: The Optical Society (OSA)].

albino and pigmented rabbits *in vivo*. **Figure 6** shows that the blood vessel diameter and blood flow in neovascularization are smaller than those of normal vessels, yet PAM can detect neovascularization and the small, irregular vascular network. At the same time, Nguyen et al. [28] have found that multi-wavelength PAM can selectively monitor and detect RVO and RNV in the rabbit retina. This has demonstrated that PAM could achieve label free imaging of microvasculature and RNV without administration of exogenous contrast agents. In addition, rabbit eyes have a similar size to human eyes, which paves the road to clinical translation of the technology.

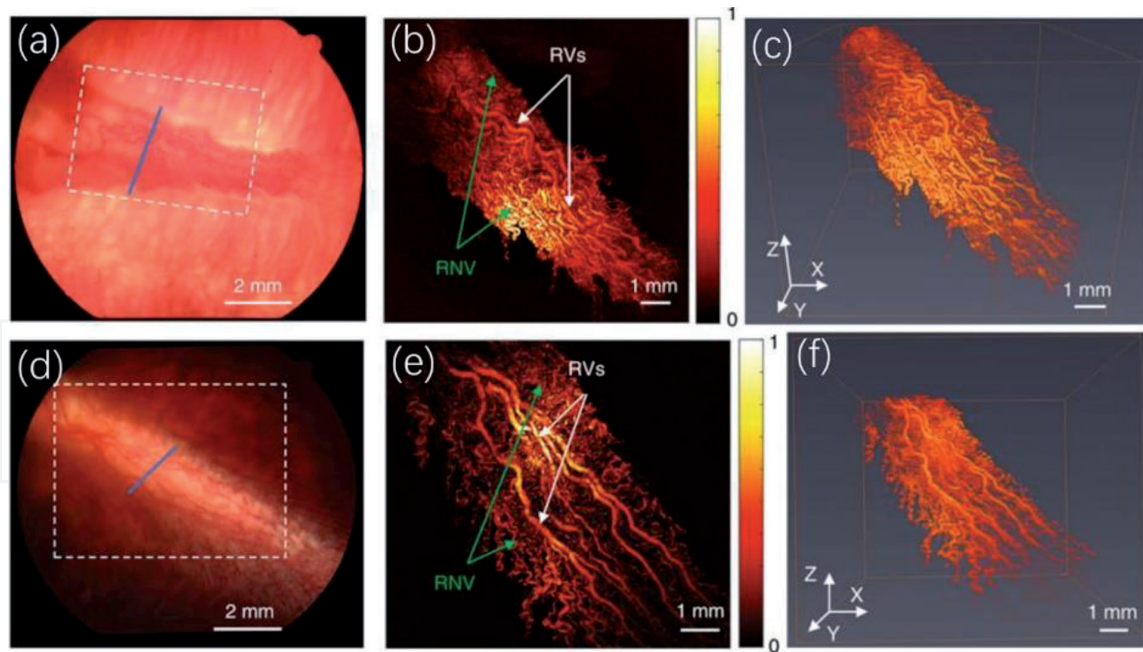


Figure 6. PA images of the retinal neovascularization. (a–c) RNV in albino rabbits. (a) Color fundus image. (b) 2D PAM image indicated by white dashed box in (a). (c) 3D reconstruction of PAM image. (d–f) RNV in pigmented rabbits. (d) Color fundus image. (e) 2D PAM image indicated by white dashed box in (d). (f) 3D reconstruction of PAM image. White arrows indicate normal retinal vessels; green arrows indicate RNV. Adapted with permission from Ref. [11] [Publisher: Springer Nature].

2.2.4 Choroidal neovascularization

Choroidal neovascularization (CNV) is characterized by the abnormal growth of new vessels originating from the choroidal vasculature and their subsequent growth under the RPE, subretinal space, or a combination of both [29]. CNV most commonly occurs in neovascular age-related macular degeneration (AMD), which is a major cause of vision loss. Dai et al. have used PAM system to investigate laser-induced rat CNV evolution. For the PAM system, the laser output wavelength was 532 nm, and the pulse energy was 60 nJ. The induced PA signals from the retina were detected by a customized ultrasonic transducer (30 MHz; bandwidth: 15 MHz). The axial and lateral resolution of PAM were 50 and 20 μm , respectively. The new capillaries growing from the choroid up to subretinal space can be distinguished as shown in Figure 7.

2.3 PA imaging in retinal metabolism

Retinal oxygen metabolic rate ($r\text{MRO}_2$) is an essential parameter in the retina and can help further understanding of some blinding diseases, such as diabetic retinopathy [31, 32] and glaucoma [33, 34]. The precise measurement of $r\text{MRO}_2$ can be critical in investigating these blinding diseases. Song et al. [35] and Liu et al. [36] have successfully determined $r\text{MRO}_2$ in rats by integrating PAOM and OCT. Obtaining $r\text{MRO}_2$ measurements required measuring retinal blood flow and $s\text{O}_2$ together. They have quantified retinal blood flow by Doppler SD-OCT, and retinal $s\text{O}_2$ by PAOM at three wavelengths (570, 578, and 588 nm). Owing to the distinct light absorption spectrum between HbO_2 and HbR , multi-wavelength imaging can assess the $s\text{O}_2$ in retinal vessels. They have calculated total retinal blood flow as 7.43 ± 0.51 and $7.38 \pm 0.78 \mu\text{L}/\text{min}$ within the venous and arterial systems, respectively. The $s\text{O}_2$ value in arterial and venous blood were 93.0 ± 3.5 and $77.3 \pm 9.1\%$, respectively. In PAOM system, they used a

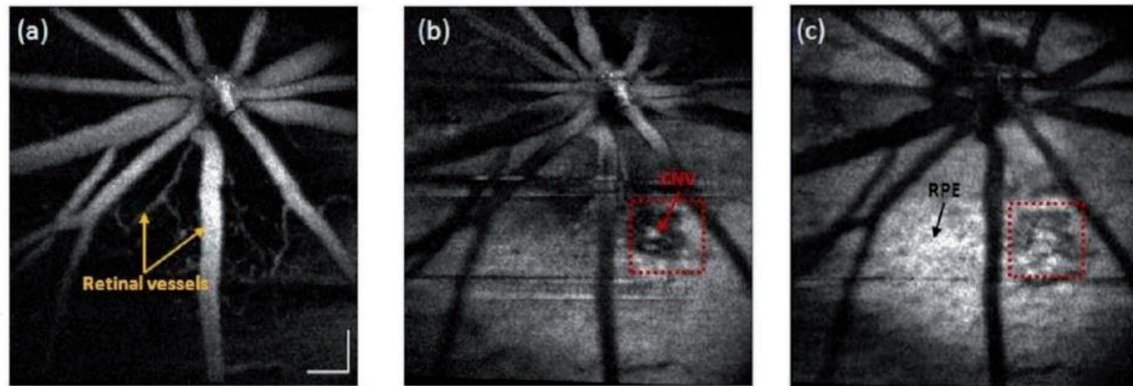


Figure 7.

PAM images at different depth in CNV rat fundus. (a) 2D enface image of anterior retinal structure. (b) 2D enface image of posterior retinal structure. (c) 2D enface image of RPE layer. Scale bars indicate 100 μm . Adapted with permission from Ref. [30] [Publisher: SPIE].

tunable laser (output laser wavelength: 570, 578, and 588 nm), the laser energy was 40 nJ/pulse. Acoustic waves were detected by an unfocused small-footprint ultrasonic transducer (40 MHz; bandwidth: 30 MHz). The lateral resolution was 20 μm , and the axial resolution was 23 μm . The study measured rMRO₂ in normal small animals. Hariri et al. [37] have demonstrated the use of PA ocular imaging (PAOI) in measuring chorioretinal oxygen saturation (CR-sO₂) gradients in New Zealand white rabbits with ocular ischemia model. The PAOI signal showed a sixfold decrease in CR-sO₂ after significant elevation of IOP during ischemia. In the PAOI, they used a tunable laser (680–970 nm), 750 and 850 nm were used to differentiate the HbO₂ and HbR. A linear array ultrasound transducer with a center frequency of 15 MHz was used to detect acoustic signals. The lateral and axial resolution were 580 and 290 μm , respectively. One limitation of the study was balancing special resolution and penetration depth. Although they could achieve much deeper penetration, they could not discriminate between the retina and the choroid, nor could they distinguish individual vessels.

2.4 PA imaging of melanin of the eye

Melanin is naturally present in the eye within the iris, ciliary body, pigmented choroid, and RPE [38]. The RPE is a single layer of epithelial cells beneath the neurosensory retina and tightly adherent to the underlying choroid. The RPE plays a crucial role in the overall health of the retina: nourishing photoreceptors and disposing of retinal waste and metabolic end products. The melanin concentration in RPE can decrease over time due to light exposure and oxidative stress [39]. RPE melanin decrease is a sign of ocular senescence and is a risk factor and a pathognomonic sign of AMD [40, 41]. To further study melanin, PAI has been used to specifically detect and quantify melanin [42].

In 2010, Silverman et al. [43] for the first time have demonstrated that PAI can acquire images of melanin in the iris in *ex vivo* pig eye. Jiang et al. [44] have designed an adaptive optics PAM (AO-PAM) system to correct the wavefront errors of the illuminating light of PAM. The lateral resolution of PAM was improved to 2.5 μm with AO. They imaged the ciliary body and the RPE layer of an *ex vivo* pig eye. In addition, the single RPE cells were first resolved by AO-PAM system (Figure 8a and b). Jiao et al. [12] have successfully acquired images of the retinal vessels and RPE in pigmented rat eyes by using integrated PAOM with OCT system with a 23 μm axial resolution. The study was the first *in vivo* demonstration of PA imaging melanin of eye. Zhang

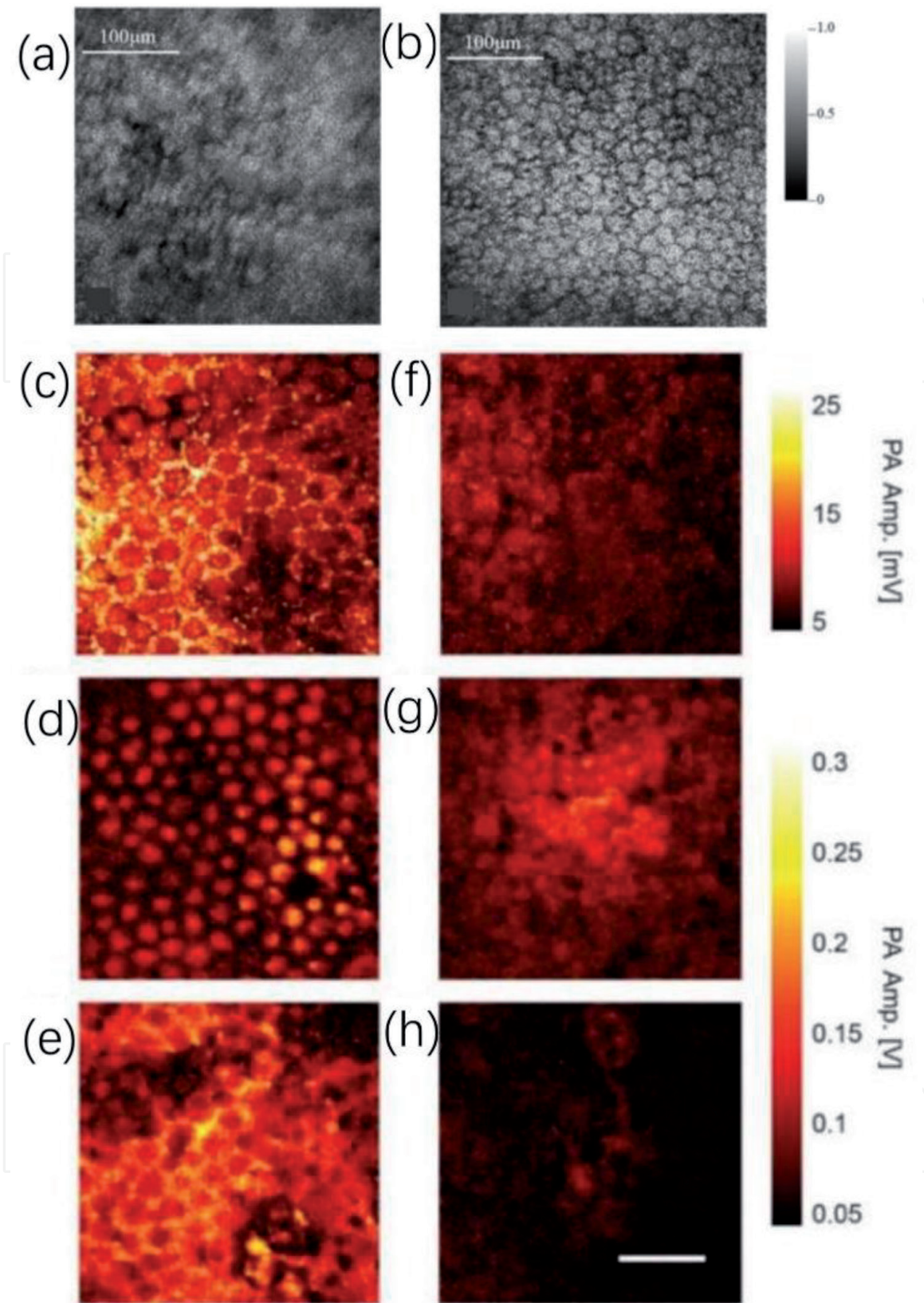


Figure 8.

PA images of melanin of the RPE. (a, b) MAP of the PAM images of the RPE of the pig eye: (a) without AO. (b) With AO. Adapted with permission from Ref. [44] [Publisher: The Optical Society (OSA)]. (c–h) PA images of porcine and human RCC. (c) PA image of porcine RCC acquired by customized piezoelectric transducer. (d, e) PA image of porcine RCC acquired by broadband MRR detector. (d) Axially segmented porcine RPE. (e) Axially segmented porcine choroid. (c, e) Are images of the same area on a single sample. (f) PA image of human RCC acquired by customized piezoelectric transducer. (g, h) PA image of human RCC acquired by homemade MRR detector. (g) Axially segmented human RPE. (h) Axially segmented human choroid. (f, h) Are images of the same area on a single sample. RCC, RPE-choroid complex. Bottom right scale bar indicates 50 μm. Adapted with permission from Ref. [45] [Publisher: The Optical Society (OSA)].

et al. [46] have combined autofluorescence (AF) with PAOM system to image the RPE melanin and lipofuscin in albino and pigmented rat eyes. Song et al. have developed a multimodal system that contains PAOM, SLO, OCT, and FA to image the eye. They have demonstrated that melanin from the RPE and choroid was able to be imaged *in vivo* in the retinal of albino and pigmented rats, [20] as well as mice [21]. To demonstrate the feasibility of NIR-light PAOM *in vivo*, Liu et al. [47] have developed a dual-wavelength (532 and 1064 nm) PAOM and further integrated it with SD-OCT to image albino and pigmented rat eyes. They found that NIR light (1064 nm) PAOM system successfully imaged RPE/choroidal melanin with good signal-to-noise ratio (SNR) in pigmented rat eyes. After that, in 2015, Liu et al. [48] have demonstrated the feasibility of an OCT-PAM system working in the NIR-light. The OCT and PAM used the same broadband light source with a center wavelength of 800 nm. This system can provide a deep-penetration depth and melanin-specific images of the retina in pigmented rats.

The above papers are qualitative studies of eye melanin by PAI. PAI also has the capability of providing a quantitative reading of melanin concentration in the eye. Shu et al. [49] have performed a Monte Carlo (MC) stimulation to investigate light propagation and energy deposition in the eye and tested the feasibility of using PAOM to quantify the RPE melanin concentration. In this study, they used PA signals from retinal blood vessels as references to measure RPE melanin variation. However, the main challenge in accurate quantification of RPE melanin concentration is to distinguish the RPE from underlying pigmented choroid. The RPE is a 10 μm thick cell monolayer and is tightly attached to the choroid, and thus a higher axial resolution of PAOM was necessary. Shu et al. [45] then have used a micro-ring resonator (MRR) detector in their PAOM system to increase the axial resolution ($<10 \mu\text{m}$). They obtained images where the RPE and choroid can be distinguished in *ex vivo* porcine and human eyes and quantified the absolute melanin concentrations in the RPE and pigmented choroid, respectively (**Figure 8c–h**).

PAI can obtain volumetric images of melanin in the eye and can quantify melanin in the RPE and the choroid. However, the technique has yet to be explored in eye disease models and the human eye, so it is unknown that how it can be used in eye research and clinic in the future.

2.5 Multimodal PA imaging system

PA imaging can obtain structural and functional imaging of the eye. PAI can also be combined with other ocular imaging devices, such as OCT, SLO, AF, AO, FA, and fundus photography. These combined multimodal platforms can compensate the weaknesses of each system and provide more comprehensive information of the eye. That would be very beneficial for investigating ocular pathology and detecting disease. For instance, with correcting wave-front errors with AO, the lateral resolution of PAM can be improved [44]. With PAM and AF combined, information on the distribution and concentration of retinal melanin and lipofuscin can be obtained *in vivo* simultaneously [46]. The most commonly integrated imaging systems combine PAI with OCT since this carries several advantages. OCT can not only acquire posterior segment anatomic information with high axial and lateral resolutions, but also can quantitatively measure retinal blood velocity and flow rate. In addition, OCT can also guide PAI, helping the PAI system image a specific region of interest in the posterior segment of the eye. Song et al. [20, 21] have developed a multimodality system which integrated PAOM, SD-OCT, AF-SLO, and FA to provide optical absorption, optical backscattering, and fluorescence properties of the retina in albino and pigmented rats and mice. Song and Liu et al. [35, 36] have quantified the $r\text{MRO}_2$ using PAOM and SD-OCT. PAOM measured the $s\text{O}_2$, and SD-OCT mapped the blood flow rate. Tian and Nguyen et al. [19, 28, 50, 51]

have used a PAM and OCT dual-modality system to acquire chorioretinal imaging and retinal neovascularization imaging in living rabbit eyes. Zhang et al. [11] have described a multimodality imaging system that combines PAM, OCT, and fluorescence microscopy (FM) to evaluate retinal angiogenesis in albino and pigmented rabbit eyes. The multimodal images can be acquired from a single imaging system and co-registered on the same image plane. Thus, ocular diseases can precisely be detected and visualized at earlier stages, resulting in improved understanding of pathophysiology, improved management, and improved monitoring of retinal treatment to prevent vision loss.

3. Limitations and future directions

3.1 Innovative laser sources for PA imaging

PA imaging can achieve anatomic information with monochromatic pulsed laser illumination. However, to acquire ocular functional information using PAI, multi-wavelength laser illuminations are required. An optical parametric oscillator (OPO) (for example, the Ekspla NT-242, pulse repetition rate 1 kHz, duration 3–6 ns, tunable wavelength range 405–2600 nm) can be used as a suitable laser source to obtain the above information. However, in multimodality systems, such as PA imaging and OCT, the two modalities can require different types of illuminations and thus separate light sources. Liu et al. [48] have used a single ultrafast laser source (pulse repetition rate 10 kHz, pulse duration 3 ns, center wavelength 800 nm; bandwidth 30 nm) to acquire melanin-specific images of *in vivo* rat retina simultaneously from PAM and OCT. However, this shared laser was limited to imaging melanin since the absorption of hemoglobin was relatively weak in the NIR range. Recently, pulse laser diodes (PLD) have been described as an alternative laser excitation source in mouse ear vascular structures [52]. In the future, one could envision PLD and other novel laser sources for PAI and multimodal imaging applied to ophthalmology.

3.2 Non-contact detection of PA signal

In reported studies to date, researchers either placed a water tank on the cornea or directly coupled an ultrasonic needle transducer with the eyelid or sclera using ultrasonic gel or balanced salt solution (BBS). Given the sensitivity of the human eye, this is not ideal for clinical application on patients. Non-contact remote sensing has been described where an interferometer is used to sense the surface displacement induced by PA ultrasound signals [53, 54]. Discovering a non-contact ultrasonic detection with both stability and sensitivity is a promising area of active investigation.

3.3 Field of view of PA imaging

The field of view (FOV) of PA imaging is limited by the ultrasound transducer. The typical scan area of reported studies has been shown in **Table 1**. For most studies, the image area was no more than 3×3 mm. The human retina area is about 10 cm^2 , so increasing the field of view would be beneficial, possibly through novel ultrasound transducer configurations or array patterns.

3.4 Speed of PA image acquisition

Several current PA imaging systems can acquire high-resolution images in <1 min. The imaging speed is limited by the laser pulse repetition rate. The image

PA system	Applications	Publication	Scanning pattern	Laser illumination	US	Speed and size	Resolution	Animal
AR-PAM	whole eye	de la Zerda [4]	Wide field illumination	W: 700/740 nm E: 0.5 mJ/cm ²	CF: 15/25 MHz B: 60%	90 min for 12 × 8 mm	L: 200/240 μm A: 83/50 μm	rabbit <i>in vivo</i> ; pig <i>ex vivo</i>
OR-PAM	Iris vasculature and sO ₂	Hu [13]	Mechanical scanning	W: 570/578 nm E: 40 nJ	CF: 75 MHz	120 min for 2 × 2 mm	L: 5 μm A: 15 μm	Swiss Webster mouse
OR-PAM	Iris vasculature	Rao [15]	Hybrid-scanning	W: 532 nm E: 60 nJ	B: 25 MHz	128 s for 4 × 4 mm	L: 3.5 μm A: <31 μm	Albino mouse
OR-PAM	Iris vasculature	Zhao [14, 55]	Mechanical scanning	W: 532 nm E: 11 mJ/cm ²	CF: 75 MHz	0.5 frame/s	L: 5.43 μm	SD rat
OR-PAM	Corneal NV; iris vasculature	Liu [16]	Mechanical scanning	W: 532 nm E: 80 nJ	CF: 10 MHz B: 80%	20 min for 3 × 3 mm	L: 2.76 μm A: 50 μm	C57BL6/J mouse
OR-PAM	Anterior vasculature	Jeon [17]	Mechanical scanning	W: 532 nm	CF: 50 MHz B: 50 MHz	3 × 3 mm	L: 3 μm	BALB/c mouse
OR-PAM	Corneal NV; blood flow and sO ₂	Kelly-Goss [18]	Mechanical scanning	W: 532/559 nm E: 50/30 nJ	CF: 35 MHz B: 70%	30 min for entire cornea	2.7 μm	Transgenic Tie2-GFP mouse
PAOM+SD-OCT	Retinal vasculature; RPE	Jiao [12]	Optical scanning	W: 532 nm E: 40 nJ	CF: 30 MHz B: 50%	2.7 s for 2 × 2 mm	L: 20 μm A: 23 μm	Long Evans rat
PAOM+SD-OCT	Retinal and choroidal vasculature	Wei [25]	Optical scanning	W: 578 nm E: 40 nJ	CF: 35 MHz B: 50%	2.7 s for 2 × 2 mm	L: 20 μm A: 23 μm	SD rat
PAOM+SD-OCT + AF-SLO + FA	Retinal and choroidal vasculature; RPE	Song [20]	Optical scanning	W: 532 nm E: 40 nJ	CF: 40 MHz B: 15 MHz	2.7 s for 2 × 2 mm	L: 20 μm A: 23 μm	Albino / pigmented rats
Fundus camera + PAOM	Retinal and choroidal vasculature	Liu [22]	Optical scanning	W: 532 nm E: 60 nJ	CF: 35 MHz B: 50%	2.7 s for 2 × 2 mm	L: 20 μm A: 23 μm	Albino / pigmented rats
PAOM+SD-OCT	Retinal and choroidal vasculature; RPE	Song [27]	Optical scanning	W: 532 nm E: 40 nJ	CF: 40 MHz B: 16 MHz	2.7 s for 2 × 2 mm	L: 20 μm A: 23 μm	Albino / pigmented rats

PA system	Applications	Publication	Scanning pattern	Laser illumination	US	Speed and size	Resolution	Animal
PAM+OCT	Retinal and choroidal vasculature	Tian [19]	Optical scanning	W: 570 nm E: 80 nJ	CF: 27 MHz B: 60%	65 s for 3 × 3 mm	L: 4.1 μm A: 37 μm	Albino rabbit
PAM+OCT + FM	Retinal vasculature and RNV	Zhang [11]	Optical scanning	W: 532 nm E: 80 nJ	CF: 27 MHz B: 60%	65 s for 3 × 3 mm	L: 4.1 μm A: 37 μm	Albino/ pigmented rabbits
PAM+OCT	RVO and RNV	Nguyen [28]	Optical scanning	Multi-wavelength E: <80 nJ	CF: 27 MHz B: 60%	65 s for 3 × 3 mm	L: 4.1 μm A: 37 μm	Albino rabbit
PAM+OCT	CNV; retinal structure; RPE	Dai [30]	Optical scanning	W: 532 nm E: 60 nJ	CF: 40 MHz B: 16 MHz	19.5 frame/s	L: 20 μm A: 50 μm	Brown Norway rat
PAOM+OCT	Retinal rMRO ₂ ; sO ₂ ; blood flow	Song [35], Liu [36]	Optical scanning	W:570/578/588 nm E: 40 nJ	CF:30 MHz B: 15 MHz	2.7 s for 2 × 2 mm	L: 20 μm A: 23 μm	SD rat
OR-PAM	Chorioretinal sO ₂	Hariri [37]	Optical scanning	W: 750/850 nm E: 8 ± 0.5 mJ	CF: 15 MHz	0.8 frame/s	L: 580 μm A: 290 μm	Albino rabbit
AO-PAM	Ciliary body, RPE melanin	Jiang [44]	Optical scanning	W:532 nm E: 40 nJ	CF:30 MHz B:50%	2.7 s for 2 × 2 mm	L: 2.5 μm A: 23 μm	Pig <i>ex vivo</i>
PAOM+AF	RPE melanin; lipofuscin	Zhang [46]	Optical scanning	W: 532 nm E: 40 nJ	CF: 30 MHz B: 50%	2.7 s for 2 × 2 mm	L: 4.5 μm A: 23 μm	Albino/ pigmented rats
PAOM+SD-OCT	RPE melanin	Liu [47]	Optical scanning	W: 1064/532 nm E: 20 nJ	CF:30 MHz B: 50%	2.7 s for 2 × 2 mm	L: 20 μm A: 23 μm	SD/Long Evans rats
Broadband PAM	RPE melanin concentration	Shu [45]	Optical scanning	W: 532 nm	MRR B: 280/27 MHz	22 s per image	A: <10 μm	Porcine/human RCCs <i>ex vivo</i>

W, wavelength; E, energy; CF, central frequency; B, bandwidth; NV, neovascularization; SD, Sprague Dawley; RPE, retinal pigmented epithelial; RNV, retinal neovascularization; RVO, retinal vein occlusion; CNV, choroidal neovascularization; rMRO₂, retinal oxygen metabolic rate; AO, adaptive optics; AF, autofluorescence; MRR, micro-ring resonator; RCC, RPE-choroid complexes.

Table 1.
Summary of key articles demonstrating photoacoustic imaging of the eye.

speed can be reduced until it depends on the ultrasound propagation time from the posterior eye. The advantage of improving imaging speed is that it will reduce motion artifacts and increase patient comfort. Ideally a clinical PA system would acquire images in less than a second to a couple seconds.

3.5 Lateral and axial resolution of PA

The lateral resolution of PA imaging is determined by the smallest achievable spot size of the illuminating light in the retina. Tian and Zhang et al. described the lateral resolution of their PAM system as $4.1\ \mu\text{m}$ [11, 19]. AO allows one to correct for ocular aberrations and has been applied to ophthalmic imaging to improve resolution. A feasibility study was conducted on the integration of AO with PAM for *ex vivo* imaging of the eye, which have improved the lateral resolution of the PAM to $2.5\ \mu\text{m}$. If one adds AO into multimodality systems, it can further improve the lateral resolution of PA imaging.

The axial resolution of PA imaging is determined by the bandwidth of the ultrasound transducer. The larger ultrasonic bandwidth will allow higher axial resolution, but with less sensitivity. Therefore, a balance is required between axial resolution and sensitivity.

3.6 Real-time PA imaging

Currently many PA images require post-image processing to display images. Further investigation of an advanced ophthalmic PA imaging system is to obtain real-time imaging.

3.7 Imaging the choroidal vasculature in pigmented animals

PA imaging is often limited to albino animals when imaging the choroid due to the high PA signal of the RPE melanin in pigmented animals. Further methods need to be developed and refined to penetrate the RPE layer and allow improved choroidal visualization. NIR light has been proposed as a solution, but further testing is needed.

3.8 Imaging ocular disease animal models

PA imaging has been demonstrated in some animal eye models to date, including mouse corneal neovascularization model, rat CNV model, and rabbit retinal neovascularization model. PA imaging needs to be further explored in more eye disease models to evaluate how the information provided by PA imaging will be used clinically in the future.

3.9 Exogenous contrast agents and theranostics

To improve PA image sensitivity and specificity, exogenous contrast agents can be utilized. PA imaging with exogenous contrast agents also allows one to extend the imaging scope to molecular imaging [56, 57]. Exogenous contrast agents for PA imaging include organic and inorganic agents. However, each agent has advantages and limitations. Organic agents (e.g., ICG) can have a limited level of contrast enhancement but a more rapid path to clinical translation [58]. Inorganic agents (e.g., gold nanoparticle (AuNP)) can offer higher contrast but a less rapid path to clinical translation due to less long-term evidence of biosafety [59, 60]. Thus, exploring suitable exogenous contrast agents with safety and high contrast can be

used for PA imaging will be meaningful in future research. In addition, theranostic agents that can be used both for diagnostic imaging and therapy, should be further refined and developed to allow for targeted therapy at the time of imaging.

3.10 Safety evaluations and clinical approval

Before PA imaging can be applied to human imaging, a thorough evaluation of laser safety is necessary. Although the reported systems compare their laser fluence to the ANSI laser safety regulations, [24] one must monitor the long-term effect of both single and multiple imaging sessions on the structure and function of the retina. In addition, regulatory approval should be sought for a clinical system so that PA can be applied to patients and diseases.

4. Conclusion

The chapter introduces the applications, recent developments, and future directions of PA imaging in the eye. It has been demonstrated that PA imaging can provide both anatomic and functional information of eye with high-resolution, high sensitivity, high-contrast, and high depth of penetration. This chapter describes the ocular structure of PA imaging including normal vasculature of the iris, retina, and choroid, neovascularization in cornea, retina, and choroid, and melanin of the RPE. This chapter summarized PA imaging to quantify the functional information of measuring the vascular sO_2 and quantifying the absolute melanin concentrations. Limitations and future directions of PA imaging of the eye are also discussed.

Acknowledgements

This research was supported by a grant from the National Eye Institute 1K08EY027458 (YMP), Fight for Sight-International Retinal Research Foundation FFSGIA16002 (YMP), unrestricted departmental support from Research to Prevent Blindness, and the University of Michigan Department of Ophthalmology and Visual Sciences, and China Scholarship Council No.201806370270.

Conflict of interest

None.

IntechOpen

Author details

Yanxiu Li^{1,2} and Yannis Mantas Paulus^{1,3*}

1 Department of Ophthalmology and Visual Sciences, University of Michigan, Ann Arbor, MI, United States

2 Department of Ophthalmology, Xiangya Hospital, Central South University, Changsha, P.R. China

3 Department of Biomedical Engineering, University of Michigan, Ann Arbor, MI, United States

*Address all correspondence to: ypaulus@med.umich.edu

IntechOpen

© 2019 The Author(s). Licensee IntechOpen. This chapter is distributed under the terms of the Creative Commons Attribution License (<http://creativecommons.org/licenses/by/3.0>), which permits unrestricted use, distribution, and reproduction in any medium, provided the original work is properly cited. 

References

- [1] Zhang HF, Maslov K, Stoica G, et al. Functional photoacoustic microscopy for high-resolution and noninvasive *in vivo* imaging. *Nature Biotechnology*. 2006;**24**:848-851
- [2] Laufer J, Zhang E, Raivich G, et al. Three-dimensional noninvasive imaging of the vasculature in the mouse brain using a high resolution photoacoustic scanner. *Applied Optics*. 2009;**48**:D299-D306
- [3] de la Zerda A, Zavaleta C, Keren S, et al. Carbon nanotubes as photoacoustic molecular imaging agents in living mice. *Nature Nanotechnology*. 2008;**3**:557-562
- [4] de la Zerda A, Paulus YM, Teed R, et al. Photoacoustic ocular imaging. *Optics Letters*. 2010;**35**:270-272
- [5] Li C, Wang LV. Photoacoustic tomography and sensing in biomedicine. *Physics in Medicine and Biology*. 2009;**54**:R59-R97
- [6] Wang LV, Hu S. photoacoustic tomography: *In vivo* imaging from organelles to organs. *Science*. 2012;**335**:1458-1462
- [7] Zhang HF, Puliafito CA, Jiao S. Photoacoustic ophthalmoscopy for *in vivo* retinal imaging: Current status and prospects. *Ophthalmic Surgery, Lasers & Imaging*. 2011;**42**(Suppl):S106-S115
- [8] Xing WX, Wang LD, Maslov K, et al. Integrated optical- and acoustic-resolution photoacoustic microscopy based on an optical fiber bundle. *Optics Letters*. 2013;**38**:52-54
- [9] Nguyen V, Paulus YM. Photoacoustic ophthalmoscopy: Principle, application, and future directions. *Journal of Imaging*. 2018;**4**:149
- [10] Liu W, Zhang HF. Photoacoustic imaging of the eye: A mini review. *Photoacoustics*. 2016;**4**:112-123
- [11] Zhang W, Li YX, Nguyen VP, et al. High-resolution, *in vivo* multimodal photoacoustic microscopy, optical coherence tomography, and fluorescence microscopy imaging of rabbit retinal neovascularization. *Light, Science & Applications*. 2018;**7**:103
- [12] Jiao S, Jiang M, Hu J, et al. Photoacoustic ophthalmoscopy for *in vivo* retinal imaging. *Optics Express*. 2010;**18**:3967-3972
- [13] Hu S, Rao B, Maslov K, et al. Label-free photoacoustic ophthalmic angiography. *Optics Letters*. 2010;**35**:1-3
- [14] Zhao H, Wang G, Lin R, et al. Three-dimensional hessian matrix-based quantitative vascular imaging of rat iris with optical-resolution photoacoustic microscopy *in vivo*. *Journal of Biomedical Optics*. 2018;**23**:1-11
- [15] Rao B, Li L, Maslov K, et al. Hybrid-scanning optical-resolution photoacoustic microscopy for *in vivo* vasculature imaging. *Optics Letters*. 2010;**35**:1521-1523
- [16] Liu W, Schultz KM, Zhang K, et al. *In vivo* corneal neovascularization imaging by optical-resolution photoacoustic microscopy. *Photoacoustics*. 2014;**2**:81-86
- [17] Jeon S, Song HB, Kim J, et al. *In vivo* photoacoustic imaging of anterior ocular vasculature: A random sample consensus approach. *Scientific Reports*. 2017;**7**:4318
- [18] Kelly-Goss MR, Ning B, Bruce AC, et al. Dynamic, heterogeneous endothelial Tie2 expression and capillary blood flow during

microvascular remodeling. Scientific Reports-UK. 2017;7:9049

[19] Tian C, Zhang W, Mordovanakis A, et al. Noninvasive chorioretinal imaging in living rabbits using integrated photoacoustic microscopy and optical coherence tomography. *Optics Express*. 2017;25:15947-15955

[20] Song W, Wei Q, Liu T, et al. Integrating photoacoustic ophthalmoscopy with scanning laser ophthalmoscopy, optical coherence tomography, and fluorescein angiography for a multimodal retinal imaging platform. *Journal of Biomedical Optics*. 2012;17:061206

[21] Song W, Wei Q, Feng L, et al. Multimodal photoacoustic ophthalmoscopy in mouse. *Journal of Biophotonics*. 2013;6:505-512

[22] Liu T, Li H, Song W, et al. Fundus camera guided photoacoustic ophthalmoscopy. *Current Eye Research*. 2013;38:1229-1234

[23] Hughes A. A schematic eye for the rabbit. *Vision Research*. 1972;12:123-138

[24] Delori FC, Webb RH, Sliney DH, et al. Maximum permissible exposures for ocular safety (ANSI 2000), with emphasis on ophthalmic devices. *Journal of the Optical Society of America. A, Optics, Image Science, and Vision*. 2007;24:1250-1265

[25] Wei Q, Liu T, Jiao SL, et al. Image chorioretinal vasculature in albino rats using photoacoustic ophthalmoscopy. *Journal of Modern Optics*. 2011;58:1997-2001

[26] Srinivasan VJ, Ko TH, Wojtkowski M, et al. Noninvasive volumetric imaging and morphometry of the rodent retina with high-speed, ultrahigh-resolution optical coherence tomography. *Investigative*

Ophthalmology & Visual Science. 2006;47:5522-5528

[27] Song W, Wei Q, Jiao S, et al. Integrated photoacoustic ophthalmoscopy and spectral-domain optical coherence tomography. *Journal of Visualized Experiments*. 2013;71:4390

[28] Nguyen V, Li YX, Zhang W, et al. Multi-wavelength, en-face photoacoustic microscopy and optical coherence tomography imaging for early and selective detection of laser induced retinal vein occlusion. *Biomedical Optics Express*. 2018;9:5915-5938

[29] Ambati J, Ambati BK, Yoo SH, et al. Age-related macular degeneration: Etiology, pathogenesis, and therapeutic strategies. *Survey of Ophthalmology*. 2003;48:257-293

[30] Dai C, Li L, Liu W, et al., editors. In vivo time-serial evaluation of laser-induced choroidal neovascularization in rats simultaneously using photoacoustic microscopy and optical coherence tomography. *Photons Plus Ultrasound: Imaging and Sensing*. SPIE. 2018

[31] Khoobehi B, Firn K, Thompson H, et al. Retinal arterial and venous oxygen saturation is altered in diabetic patients. *Investigative Ophthalmology & Visual Science*. 2013;54:7103-7106

[32] Hardarson SH, Stefansson E. Retinal oxygen saturation is altered in diabetic retinopathy. *The British Journal of Ophthalmology*. 2012;96:560-563

[33] Olafsdottir OB, Hardarson SH, Gottfredsdottir MS, et al. Retinal oximetry in primary open-angle glaucoma. *Investigative Ophthalmology & Visual Science*. 2011;52:6409-6413

[34] Vandewalle E, Pinto LA, Olafsdottir OB, et al. Oximetry in glaucoma: Correlation of metabolic change with

structural and functional damage. *Acta Ophthalmologica*. 2014;**92**:105-110

[35] Song W, Wei Q, Liu WZ, et al. A combined method to quantify the retinal metabolic rate of oxygen using photoacoustic ophthalmoscopy and optical coherence tomography. *Scientific Reports—UK*. 2014;**4**:6525

[36] Liu WZ, Zhang HF. Noninvasive *in vivo* imaging of oxygen metabolic rate in the retina. In: *Conference Proceedings: Annual International Conference of the IEEE Engineering in Medicine and Biology Society. IEEE Engineering in Medicine and Biology Society. Annual Conference*. 2014. pp. 3865-3868

[37] Hariri A, Wang J, Kim Y, et al., editors. *In Vivo Photoacoustic Imaging of Chorioretinal Oxygen Gradients*. *Journal of Biomedical Optics*. SPIE; 2018

[38] Weiter JJ, Delori FC, Wing GL, et al. Retinal pigment epithelial lipofuscin and melanin and choroidal melanin in human eyes. *Investigative Ophthalmology & Visual Science*. 1986;**27**:145-152

[39] Schmidt SY, Peisch RD. Melanin concentration in normal human retinal pigment epithelium. Regional variation and age-related reduction. *Investigative Ophthalmology & Visual Science*. 1986;**27**:1063-1067

[40] Kanis MJ, Berendschot TT, van Norren D. Influence of macular pigment and melanin on incident early AMD in a white population. *Graefe's Archive for Clinical and Experimental Ophthalmology*. 2007;**245**:767-773

[41] Berendschot TT, Willemsse-Assink JJ, Bastiaanse M, et al. Macular pigment and melanin in age-related maculopathy in a general population. *Investigative Ophthalmology & Visual Science*. 2002;**43**:1928-1932

[42] Lapierre-Landry M, Carroll J, Skala MC. Imaging retinal melanin: A review of current technologies. *Journal of Biological Engineering*. 2018;**12**:29

[43] Silverman RH, Kong F, Chen YC, et al. High-resolution photoacoustic imaging of ocular tissues. *Ultrasound in Medicine & Biology*. 2010;**36**:733-742

[44] Jiang M, Zhang X, Puliafito CA, et al. Adaptive optics photoacoustic microscopy. *Optics Express*. 2010;**18**:21770-21776

[45] Shu X, Li H, Dong BQ, et al. Quantifying melanin concentration in retinal pigment epithelium using broadband photoacoustic microscopy. *Biomedical Optics Express*. 2017;**8**:2851-2865

[46] Zhang X, Zhang HF, Puliafito CA, et al. Simultaneous *in vivo* imaging of melanin and lipofuscin in the retina with photoacoustic ophthalmoscopy and autofluorescence imaging. *Journal of Biomedical Optics*. 2011;**16**:080504

[47] Liu T, Wei Q, Song W, et al. Near-infrared light photoacoustic ophthalmoscopy. *Biomedical Optics Express*. 2012;**3**:792-799

[48] Liu X, Liu T, Wen R, et al. Optical coherence photoacoustic microscopy for *in vivo* multimodal retinal imaging. *Optics Letters*. 2015;**40**:1370-1373

[49] Shu X, Liu W, Zhang HF. Monte Carlo investigation on quantifying the retinal pigment epithelium melanin concentration by photoacoustic ophthalmoscopy. *Journal of Biomedical Optics*. 2015;**20**:106005

[50] Tian C, Zhang W, Nguyen VP, et al. Novel photoacoustic microscopy and optical coherence tomography dual-modality chorioretinal imaging in living rabbit eyes. *Journal of Visualized Experiments*. 2018;**8**:132

- [51] Nguyen V, Li YX, Aaberg M, et al. *In vivo* 3D imaging of retinal neovascularization using multimodal photoacoustic microscopy and optical coherence tomography imaging. *Journal of Imaging*. 2018;**4**:150
- [52] Wang T, Nandy S, Salehi HS, et al. A low-cost photoacoustic microscopy system with a laser diode excitation. *Biomedical Optics Express*. 2014;**5**:3053-3058
- [53] Wang Y, Li CH, Wang RK. Noncontact photoacoustic imaging achieved by using a low-coherence interferometer as the acoustic detector. *Optics Letters*. 2011;**36**:3975-3977
- [54] Rousseau G, Blouin A, Monchalain JP. Non-contact photoacoustic tomography and ultrasonography for tissue imaging. *Biomedical Optics Express*. 2012;**3**:16-25
- [55] Chen J, Lin R, Wang H, et al. Blind-deconvolution optical-resolution photoacoustic microscopy *in vivo*. *Optics Express*. 2013;**21**:7316-7327
- [56] Luke GP, Yeager D, Emelianov SY. Biomedical applications of photoacoustic imaging with exogenous contrast agents. *Annals of Biomedical Engineering*. 2012;**40**:422-437
- [57] Yang XM, Stein EW, Ashkenazi S, et al. Nanoparticles for photoacoustic imaging. *Wiley interdisciplinary reviews. Nanomedicine and Nanobiotechnology*. 2009;**1**:360-368
- [58] Zanganeh S, Li H, Kumavor PD, et al. Photoacoustic imaging enhanced by indocyanine green-conjugated single-wall carbon nanotubes. *Journal of Biomedical Optics*. 2013;**18**:096006
- [59] Li W, Chen X. Gold nanoparticles for photoacoustic imaging. *Nanomedicine (London, England)*. 2015;**10**:299-320
- [60] Mallidi S, Larson T, Tam J, et al. Multiwavelength photoacoustic imaging and plasmon resonance coupling of gold nanoparticles for selective detection of cancer. *Nano Letters*. 2009;**9**:2825-2831